THE UNIVERSITY of EDINBURGH

Edinburgh Research Explorer

A Reconfigurable 3-D-Stacked SPAD Imager With In-Pixel Histogramming for Flash LIDAR or High-Speed Time-of-Flight Imaging

Citation for published version:
Hutchings, SW, Johnston, N, Gyongy, I, Al Abbas, T, Dutton, NAW, Tyler, M, Chan, S, Leach, J & Henderson, RK 2019, 'A Reconfigurable 3-D-Stacked SPAD Imager With In-Pixel Histogramming for Flash LIDAR or High-Speed Time-of-Flight Imaging', *IEEE Journal of Solid-State Circuits*, vol. 54, no. 11, pp. 2947-2956. https://doi.org/10.1109/JSSC.2019.2939083

Digital Object Identifier (DOI):
10.1109/JSSC.2019.2939083

Link:
Link to publication record in Edinburgh Research Explorer

Document Version:
Peer reviewed version

Published In:
IEEE Journal of Solid-State Circuits

General rights
Copyright for the publications made accessible via the Edinburgh Research Explorer is retained by the author(s) and / or other copyright owners and it is a condition of accessing these publications that users recognise and abide by the legal requirements associated with these rights.

Take down policy
The University of Edinburgh has made every reasonable effort to ensure that Edinburgh Research Explorer content complies with UK legislation. If you believe that the public display of this file breaches copyright please contact openaccess@ed.ac.uk providing details, and we will remove access to the work immediately and investigate your claim.

Download date: 17. Nov. 2026

A Reconfigurable 3D-stacked SPAD Imager with In-Pixel Histogramming for Flash LIDAR or High Speed Time of Flight Imaging

Sam W. Hutchings, Nick Johnston, Istvan Gyongy, Tarek Al Abbas, Neale A. W. Dutton, Max Tyler, Susan Chan, Jonathan Leach and Robert K. Henderson, *Senior Member, IEEE*

***Abstract*—A 256 x 256 single photon avalanche diode (SPAD) sensor integrated in a 3D-stacked 90nm 1P4M/40nm 1P8M process is reported for flash light detection and ranging (LIDAR) or high speed direct time of flight (ToF) 3D imaging. The sensor bottom tier is composed of a 64x64 matrix of 36.72 μm pitch modular photon processing units which operate from shared 4x4 SPADs at 9.18 μm pitch and 51% fill-factor. A 16 x 14-bit counter array integrates photon counts or events to compress data to 31.4 Mbps at 30 fps readout over 8 I/O operating at 100 MHz. The pixel-parallel multi-event TDC approach employs a programmable internal or external clock for 0.56 ns to 560 ns time bin resolution. In conjunction with a per-pixel correlator, the power is reduced to less than 100 mW in practical daylight ranging scenarios. Examples of ranging and high speed 3D TOF applications are given.**

Index Terms—**3-D imaging, CMOS, direct time of flight (dTOF), histogramming, image sensor, light detection and ranging (LiDAR), single photon avalanche diodes (SPADs), time-to-digital converter (TDC), TDC sharing architecture, TOF.**

I. Introduction

LIGHT Detection and Ranging (LIDAR) applications pose extremely challenging dynamic range (DR) requirements on optical ToF receivers due to laser returns affected by the inverse square law over 2-3 decades of distance, diverse target reflectivity and high solar background [1][2]. Integrated CMOS SPADs have a native DR exceeding 140dB, typically extending from the noise floor of few counts per second (cps) to 100's Mcps peak rate [3]. To deliver this DR to downstream digital signal processing (DSP), large SPAD time-resolved imaging arrays must count and time billions of single photon events per second demanding massively parallel on-chip pixel processing to achieve practical I/O power consumption and data rates.

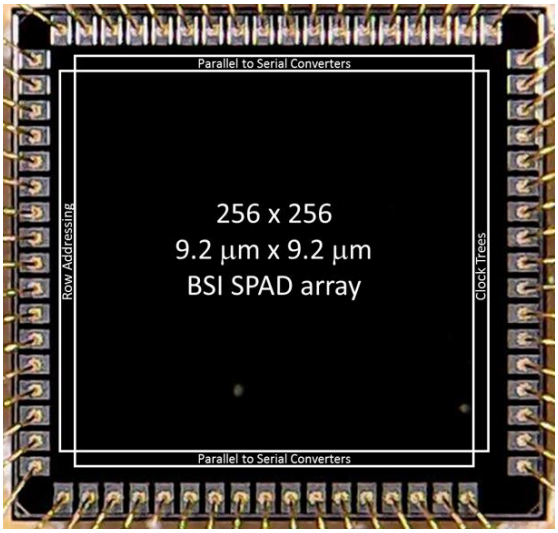

Fig. 1. Sensor micrograph.

Hybrid Cu-Cu bonding offers a mass-manufacturable platform to implement these sensors by providing high fill-factor SPADs optimized for NIR stacked on dense nanoscale digital processors [4][5][6].

While some of the key challenges to practical SPAD widefield imagers are resolved by advanced manufacturing technologies others must be addressed by design innovation. In particular, achieving simultaneously high spatial/temporal resolution and dynamic range at low power consumption and I/O data rates is especially challenging. The new design freedom offered by 3D-stacking of SPAD arrays has inspired a number of novel stacked sensor architectures involving pixel-level histogramming, on-chip peak detection and TDC/processor resource sharing [7][8][9]. However, so far none has entirely managed to balance satisfactorily these conflicting factors, either consuming high power or generating high volumes of timestamp data.

This paper presents the first large imaging array of compact,

This work was supported by the Engineering and Physical Sciences Research Council through the Quantum Hub in Quantum Enhanced Imaging EP/M01326X/1 and UKRI Innovation Fellowship EP/S001638/1. We are grateful to STMicroelectronics and the ENIAC-POLIS project for chip fabrication. The EPSRC CDT in Intelligent Sensing and Measurement, Grant Number EP/L016753/1 supported Sam Hutchings' work.

Robert K. Henderson, Nick Johnston, Istvan Gyongy and Tarek Al Abbas are with School of Engineering, University of Edinburgh, Kings Buildings, Mayfield Road, Edinburgh, EH9 3JL, UK (e-mail: Robert.Henderson@ed.ac.uk). Max Tyler, Susan Chan, Jonathan Leach are with Heriot Watt University, Institute of Photonics and Quantum Sciences, Edinburgh, U.K. Neale A.W. Dutton is with STMicroelectronics, Tanfield, Edinburgh, EH3 5DA, UK.

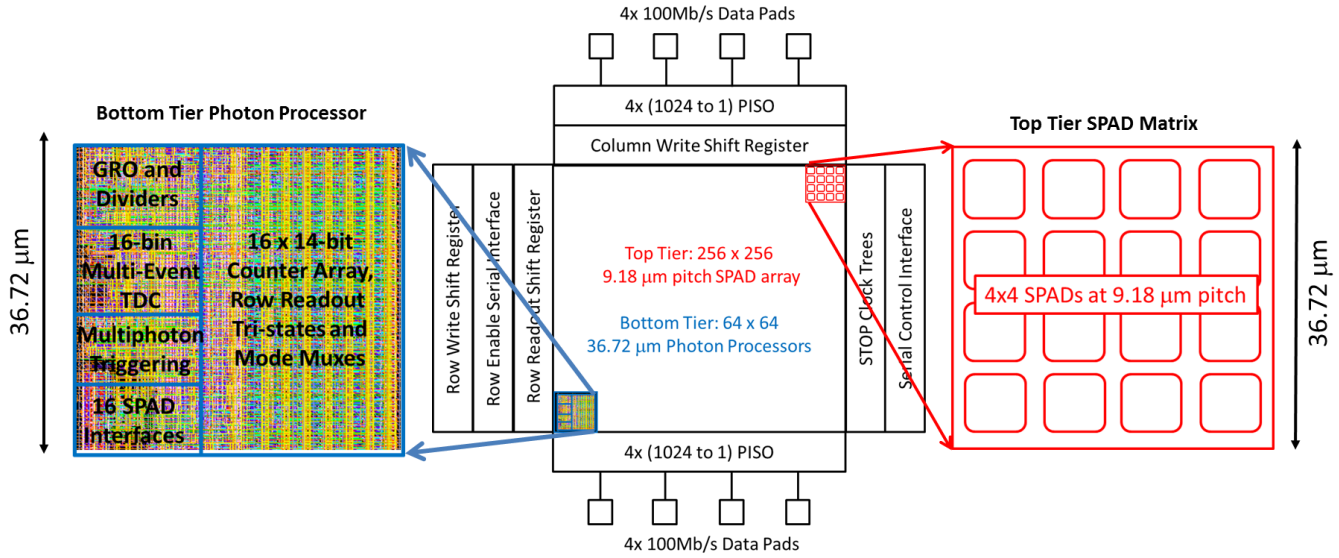

Fig. 2. Sensor architecture showing pixel layout on bottom tier (left) and SPAD layout on top tier (right).

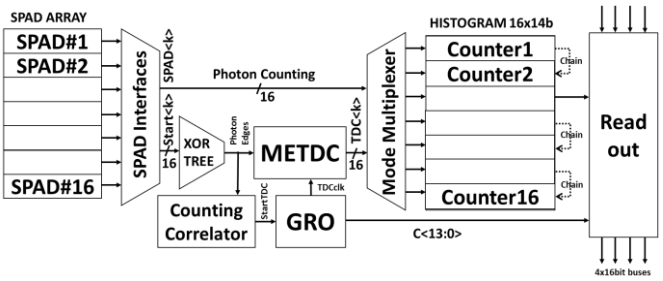

Fig. 3. Pixel architecture

reconfigurable SPAD time-resolved pixels in a 3D-stacked 90nm 1P4M/40nm 1P8M CMOS technology. We address pixel power consumption by employing an in-pixel correlator which triggers TDC activity only on multiple photon detections within nanosecond timescales most likely to occur from short laser pulses rather than background light or dark count [10]. In addition, power is conserved by a selectable internal/external TDC clock generation which uses high resolution internal TDC power sparingly in small time ranges to refine coarse but lower power range estimates from external TDC clocking. Dynamic range is tackled by in-pixel integration of photon counts or events in a counter bank, with TDC throughput enhanced by a multi-event shift-register approach.

II. Sensor Design

Fig. 1 shows a chip micrograph indicating the positions of the main functional blocks. Little circuit detail is visible because of the backside illuminated silicon of the top tier. Fig. 2 shows the chip organization, 8 I/O pads generate a modest 31.6 Mbps of pixel data at the targeted 30fps (a maximum of 800 Mbps at 760 fps). Pixels are read out by a pairwise rolling scheme from the center outwards over 256 16-bit column buses. Two exposure schemes are employed, either rolling pairwise readout while all other rows are in integration or a global shutter scheme where all rows are in integration which is then suspended before readout. A uniform top tier BSI matrix of 256 x 256 pwell/deep-nwell SPADs at 9.18 µm pitch with 51% fill-factor occupies the top tier [2][4]. The SPAD has median dark count rate of 20 cps at 1.5 V excess bias and peak PDP of 28% at 615 nm falling to around 5% at 900nm [11]. In the bottom-tier a 64 x 64 matrix of modular pixel processors at 36.72 µm pitch is integrated in 40nm CMOS technology. A dense custom layout approach employing area-optimized d-type flip-flops has been employed to allow ~40 M transistors to be integrated under the 5.38 mm^2 focal plane.

Operating Mode	Key Signals	Time Resolution	Photons/ Pixel/ Frame	Resolution	Application
Single Photon Counting (SPC)	SPCMode=1, SPAD<k>	1ms	16x16384	256x256	Rolling Shutter Intensity Imaging
Windowed/Global Shutter (GS) Photon Counting	SPCMode=0, SPAD<k>, STOP=1, Window, ToggleEn=1	5ns	16x16384	256x256	Global Shutter Imaging, Indirect Time of Flight, Frequency-Domain Fluorescence Lifetime
Windowed High Dynamic Range (HDR) Single Photon Counting	SPCMode=0, SPAD<k>, STOP=1, Window, ToggleEn=1, Chain=1	5ns	16x256M	256x64	High Dynamic Range Imaging, HDR Indirect Time of Flight
Single Shot Timestamping	SPCMode=0, Start<k>, ToggleEn=1, Window, StartTDC	35ps/14-bit	1	64x64	TCSPC, Fluorescence Lifetime Imaging, Flash LIDAR
Multi-event Histogramming	SPCMode=0, Start<k>, ToggleEn=1, Window, PhotonEdges, StartTDC, TDC<15:0>	560ps-560ns/bin	16x16384	64x64	Flash LIDAR, 3D Time of Flight Imaging, Fluorescence Lifetime Imaging
First photon	SPCmode=0, ToggleEn=0, Window, STOP, SPAD<k>	10ns-1ms	16	256x256	Fluorescence Correlation Spectroscopy, Quantum Imaging

Table. 1. Sensor operating modes

The reconfigurable pixel architecture is shown in Fig. 3. A 16 x 14b ripple counter array and mode multiplexer allow the sensor to operate in a number of imaging modalities which are summarized in Table 1 including their key signals, resolutions and main applications. The counter bank can be re-purposed for either photon counting or as time bins for in-pixel histogramming. The full resolution 256x256 of the sensor is available in single photon counting (SPC) mode with a bit depth commensurate with common full well depths (and hence SNR) in conventional pinned photodiode pixels (16384). Photon counting modes can be combined with windowing or electrical gating of the SPADs suppress background or provide indirect time of flight or frequency domain lifetime imaging. This

function also provides an option to operate the pixel in global shutter exposure (with zero parasitic light sensitivity) while the default is a high temporal aperture (127/128) rolling shutter exposure.

A gated ring oscillator (GRO) can be used for either single shot timestamping of single photons for precise but low throughput time correlated single photon counting (TCSPC).). This mode finds use in scientific imaging or long range LIDAR where the 38ps time resolution and 143 ns range (tunable to 500ns) are suited to common distances and fluorophores. The same GRO can be employed as the frequency reference for an in-pixel histogramming mode for short range time of flight with high photon timing throughput at a modest I/O rate. Here the time resolution is coarse (560ps upwards in factors of 2) but finer depth is recovered by peak centroiding. In microscopy applications the bin size is still sufficient for common fluorescence lifetimes (few ns decay time). The same GRO can be employed as the frequency reference for an in-pixel histogramming mode for short range time of flight with high photon timing throughput at a modest I/O rate. The various modes generally involve a tradeoff of spatial and temporal resolution where the counters and GRO are shared between all 16 SPADs via an XOR tree. Alternatively dynamic range and counter depth are traded for spatial resolution by chaining counters or sharing the timing functions of the multi-event TDC (METDC) or GRO. A counting correlator can be applied with a variable threshold to suppress background and save power in all timing modes. Use of an external clock for multi-event histogramming or STOP clock in single shot timestamping offer longer time ranges at lower power consumption than the in-pixel GRO.

Switching between the various modes can be achieved either instantaneously where the control signals are available on pads or within around 320ns where reprogramming of the serial interface is required. Rapidly alternating between say multi-event histogramming for 3D imaging and SPC mode has been proven very useful to combine the lower spatial resolution depth estimation with improved spatial intensity information [12]. All operating modes apply globally to the whole array and cannot be reprogrammed on a per-pixel basis.

In SPC mode, the 16 SPADs can be multiplexed directly to a bank of 16 14-bit counters realizing shot noise limited digital photon counting imaging with a 16384 photon full-well capacity (84dB DR). GS-HDR modes are realised by chaining the counters into 8 x 28b whilst binning groups of 4 SPADs allowing 256M photons per SPAD to be counted in an exposure period with a 64 x 256 spatial resolution. Binning SPADs in groups of 4 (rather than 2 for higher spatial resolution) was chosen to allow a ping-pong global-shutter indirect time of flight mode. This is of value to allow the imager to operate over long exposure times (1s) without the possibility of counter saturation even at the peak SPAD event rate of 200 Mcps. The same 16 counters are repurposed for LIDAR or 3D imaging as histogram bins for direct time of flight operation where the resolution is now 64x64 pixels. In this case a tradeoff is made between temporal and spatial resolution to allow on-chip integration of timed photons, greatly reduced I/O rates and extended dynamic range,

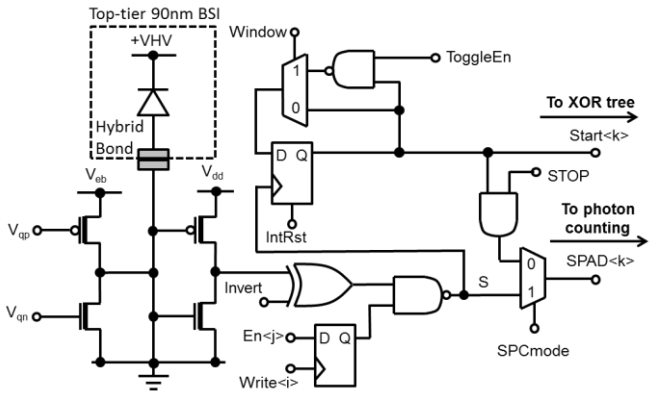

Fig. 4. SPAD interfaces

Fig. 4 shows the SPAD interface circuit which has been designed to be highly area-efficient and multi-functional. Only four thick oxide devices are employed to perform passive quenching or gating of the SPAD as well as level shifting from the excess bias voltage V_{eb} (up to 3.3V) to the logic voltage V_{dd} of 1.1V. The interface is also agnostic to the SPAD polarity for compatibility to future top tier detector generations which may integrate n-on-p or p-on-n SPAD structures. The combination of external global V_{qp} and V_{qn} voltages and the Invert signal allow selection of either NMOS or PMOS quench transistors and time gating. An enable SRAM allows masking of noisy detectors. Two 16-bit datapaths (Fig. 3) connect the SPAD interface circuits to the pixel counter array, implementing parallel photon counting or timing using the *SPAD(k)* or *Start(k)* signals respectively. The *Start(k)* signals act as a start trigger for the in-pixel TDC which can operate in either single shot timestamping mode or multi-event histogramming mode. When *ToggleEn* is low, only the first photon within a frame exposure time will be time-stamped by the single shot TDC. This first photon in the k^{th} SPAD is encoded as a rising edge of *Start(k)* and combined by the XOR tree and correlator as *PhotonEdges* to initiate single shot timestamping operation (Fig. 5). Alternatively if the *SPAD(k)* outputs are used in conjunction with *SPCmode*=0, the counters can be used to count STOP edges to provide per-SPAD photon arrival macro-times. A macro-time is the coarse time offset from the start of frame exposure to detection of the first photon arrival, as a count of the number of laser cycles (or STOP clock cycles). A macro time can be combined with a micro-time (the fine TDC timestamp of the photon arrival) to generate a precise time arrival estimate of the first photon in a frame for every pixel.

When *ToggleEn* is high, multiple photons can now be time converted per laser cycle by the multi-event TDC and integrated in the histogram memory over many laser cycles. Photon arrivals are encoded on both rising and falling edges of *Start(k)*. The 16 *Start(k)* toggling outputs are then mixed via an XOR tree and correlator to a single sequence *PhotonEdges* which is passed to the multi-event TDC (METDC) (Fig. 5).

PhotonEdges is processed by a counter-based correlator circuit (Fig. 5) which continually counts photons from the first rising edge received in each a laser cycle. A threshold of 1, 2, 4, 8 photons occurring within a 0.5-10ns delay time (adjustable

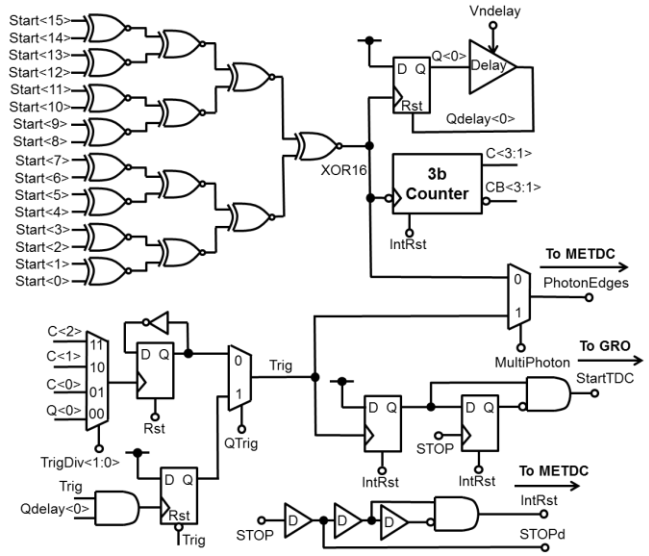

Fig. 5. Pixel event combining and counter-based correlator

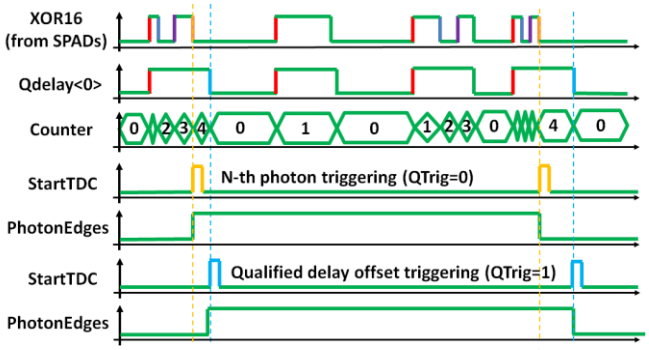

Fig. 6. Timing diagram showing the two operating modes of the counter based correlator (a) triggering on the n-th photon arrival QTrig=0 (b) n-photon qualified triggering from a fixed delay offset of first photon.

by current starving voltage (V_{ndelay}) will generate an output trigger to start the gated ring oscillator (GRO). This circuit saves power by only activating the GRO if there is a highly correlated burst of photons likely to belong to a laser return while suppressing uncorrelated background light. An example of the timing of this circuit is shown in Fig. 6. When *Qtrig* is asserted, it enables a qualified trigger as the delayed first photon in the burst provided that the threshold has been met. Although this creates a histogram with a time-offset, the matching of the V_{ndelay} controlled current starving circuit is sufficient to allow acceptable uniformity and simple offset correction. The toggling trigger sequence can also be generated on multiple bursts for use in the METDC.

The METDC is based on the architecture presented in [13] operating with a shift-register delay chain to allow digitally programmable time bin resolution over a wide temporal range. This architecture allows time digitization of up to 16 photons per laser cycle, or 1 photon per SPAD per laser cycle. Time bin resolution is set over a range 0.56 ns to 560 ns by *TDCclk* by selection of a divided phase of the GRO. This clock starts only on the first trigger (single or multi-photon) for power saving. The 14b GRO TDC shown in Fig. 7 is adjustable by the V_{ddro} voltage over a full-scale range of 560 ns to 1.6 µs for a 35 ps to 100 ps LSB resolution, matched to common automotive LIDAR ranges. Alternatively, for longer distance range *TDCclk* can

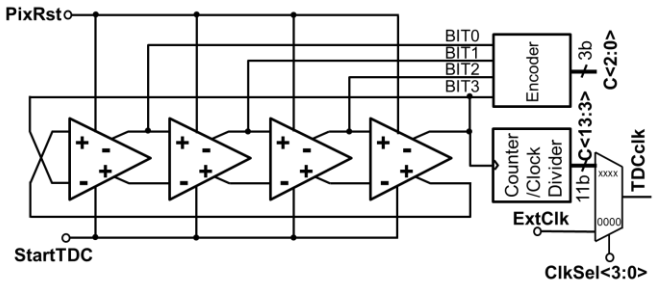

Fig. 7. Gated ring oscillator which can operate either as a coarse-fine single shot TDC or as a programmable clock source for the multi-event TDC (METDC). Notice also the option to multiplex in a global external clock for longer time intervals.

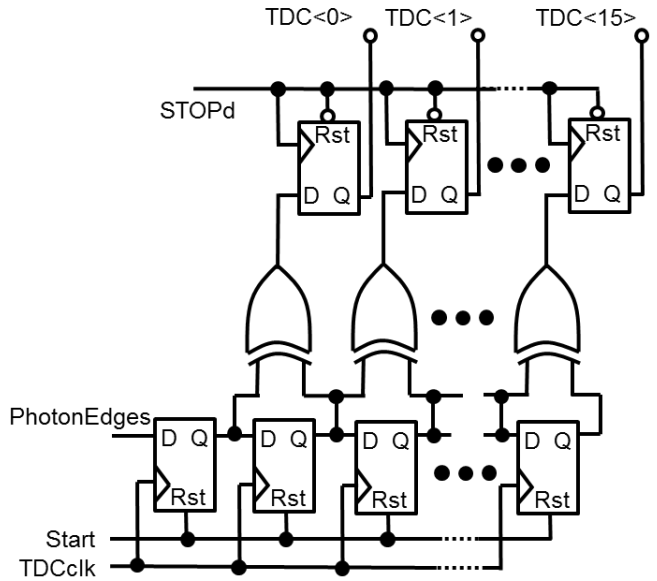

Fig. 8. 16-bin clocked shift-register multi-event TDC (METDC).

connected to a lower frequency global external clock *ExtClk*. GRO TDCs are attractive because they offer high time resolution and low average power consumption proportional to photon flux. However they also feature high peak power consumption, accumulated jitter and mismatch. We propose here to operate the GRO TDCs only for short time intervals (50-100ns) where these disadvantages are minimized. For longer time intervals such as required by LIDAR operating over 100's of meters or kilometers, the global *ExtClk* generated by an on-chip PLL would be favored. In this case long term accumulation of jitter will be eliminated by the PLL although a constant average power consumption will be drawn by clock distribution to the array with *Extclk* typically in the range of 10's to 100's of MHz.

TDCclk is then used to clock a 16-stage shift register within the METDC (Fig. 8) setting the bin time duration of the resulting 16-bin histogram. The operation of this circuit is illustrated in Fig. 9 using a simplified example for a circuit with only 4-bins. The XOR-tree output from the SPADs toggles twice the edges representing 2 photon arrivals from amongst the 16-SPADs. The GRO is started by the first of these and oscillates for around 2 and a half periods producing 3 rising edges which clock the shift register onwards three times. The initial reset state of the METDC in Fig. 9b shows 0 states at all

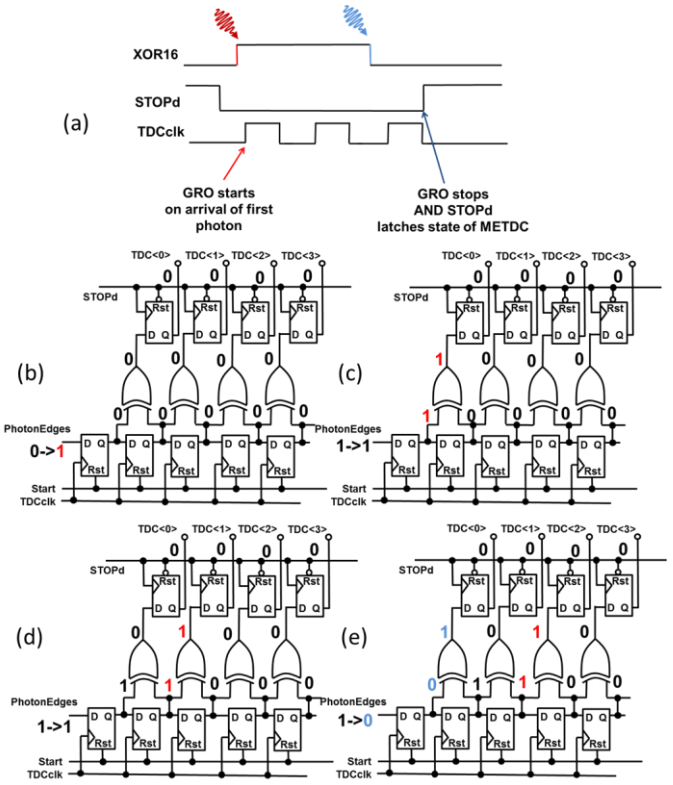

Fig. 9. Simplified timing example of multi-event histogramming operation with a 4-bin TDC, three clock cycles and two photon arrivals (a) timing diagram (b) initial state (c) after first clock edge (d) after second clock edge (e) after third clock edge and rising edge of *STOPd*.

internal nodes. After the first *TDCclk* edge the high state of *XOR16* is latched into the first position in the shift register (Fig. 9c). On the second *TDCclk* edge this 1 moves one position forward and another 1 is introduced as no new photon has arrived (Fig, 9d). On the third clock edge the *XOR16* has toggled from the second photon and a 0 is introduced (Fig. 9e). The chain of XORs pick out these transitions in the shift register generating a multiple hot code. The positions of ones in this code represent the time offset in *TDCclk* cycles of photon arrivals from the *STOPd* clock which is synchronized to the pulsed light source. On the high transition of the STOPd clock this multiple hot code is latched as *TDC<3:0>* which is multiplexed into the clock inputs of an array of counters forming a 4-bin histogram. The bits *TDC<0>* and *TDC<2>* which transition high increment their respective histogram bins in parallel. Thus multiple photons can be recorded within one laser cycle compared to a more conventional TDC which places a single timestamp in a histogram memory per laser cycle.

Readout of the 16 x 14-b counter array is accomplished in either a rolling shutter or global shutter approach. The pixel reads out over 4 x 16-bit parallel buses which is subsequently serialized over 8 I/O pads operating at 100 MHz. Operating at 30 fps the sensor produces a very modest 31.4 Mbps of data which is readily processed to extract histogram peak locations by an external FPGA. A frame rate of 760fps has been achieved in global shutter mode although a glitch in the token-passing shift register currently limits the sensor to access only half the available image resolution.

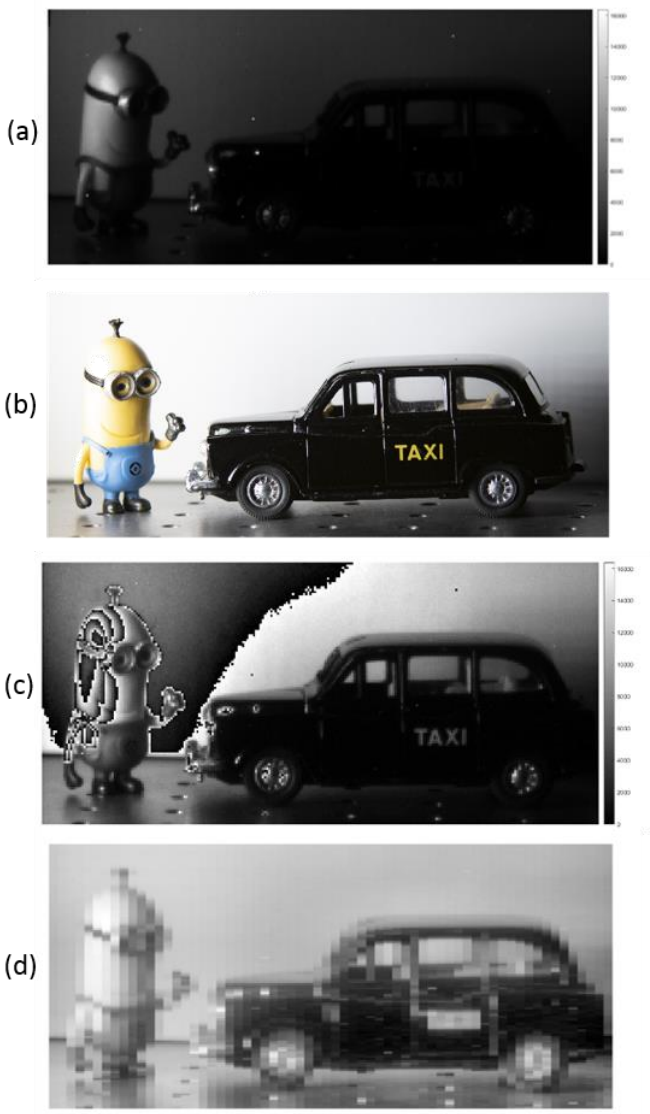

Fig. 10. SPC mode: (a) 1klux illumination 14b image; (b) side-illuminated 100klux scene with Nikon camera; (c) 100klux illumination 14b code roll-over image; (d) 100klux illumination 28b image with 4× pixel binning

III. Sensor Characterization

Fig. 10a-d shows a series of 33ms exposure global shutter photon counting images taken using a white LED array lamp to illustrate the high dynamic range of the sensor. In 1klux lighting the 14b counters do not saturate (Fig. 10a). The light level is increased to 100klux showing saturation and clipping in the Nikon reference image (Fig. 10b). In the same illumination conditions the 14b counters rollover and corrupt the image in the top left corner (Fig. 10c). Detail in this area is recovered in the tone-mapped 28b photon counting image albeit at four times lower image resolution (Fig. 10d). No electronic masking or image post-processing has been applied to remove high DCR pixels in Fig. 10.

The HDR global shutter mode is insensitive to parasitic light as the frame is stored in digital form. A DR of 120 dB is seen in the photon transfer curve in Fig. 11 with peak count rates of

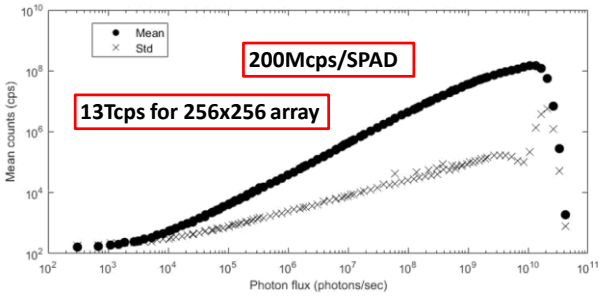

Fig. 11 Photon transfer curve in HDR mode

200 Mcps/SPAD or 13 Tcps for the whole array. We believe this is the first time the full native SPAD dynamic range is available in a video rate widefield image sensor.

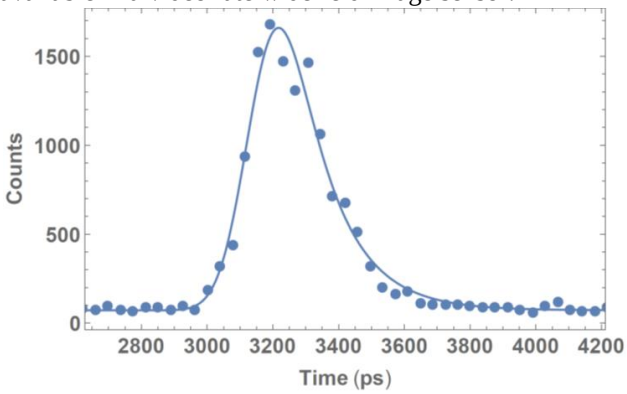

Fig. 12. Impulse response function in single shot TDC mode (170ps FWHM)

Fig, 12 shows an impulse response function (IRF) in single shot TDC mode captured using a 775 nm Coherent Chameleon Ultra laser operating at 80 MHz. The TDC resolution is 38ps and the mean FWHM across the array including laser, SPAD and system jitter is 277 ps with a standard deviation of 30 ps.

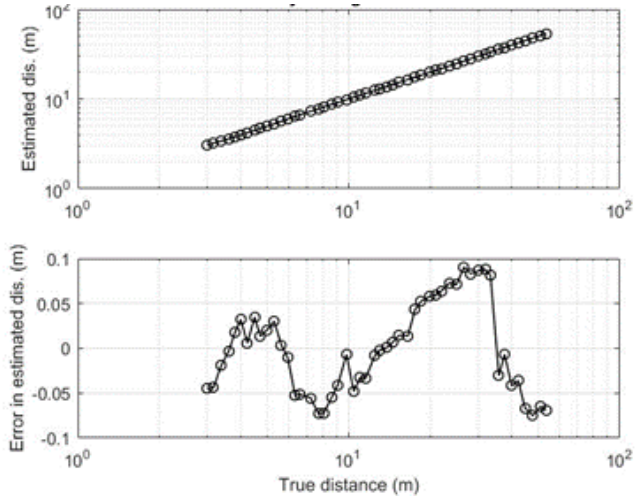

Fig. 13. Linearity in single shot TDC mode

Fig. 13 shows the linearity of the single shot TDC operating in direct ToF as +/-10 cm over a 50 m range. These latter data were obtained with a 671 nm Picoquant pulsed laser coupled into a 100 μm multimode fiber and passed through a 15 mm lens to flood illuminate the scene. The pulse duration of the laser was ~100 ps, the repetition rate was 1.9 MHz, and after the fibre and imaging lens, the laser power was measured to be 1.8 mW.

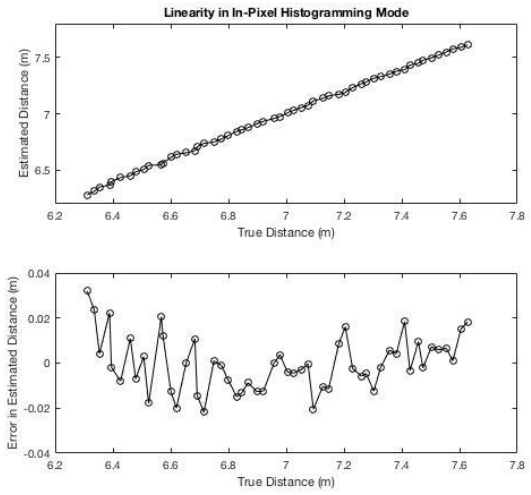

Fig. 14. Linearity in multi-event histogramming mode

Fig. 14 shows distance accuracy in multi-event histogramming mode improved over that expected from the 560 ps bin size by spreading the pulse energy over bins and performing centroiding around the peak. As the linearity of the METDC depends primarily on clock intervals and not delay cell matching, the INL and DNL are far in excess of the 4-b level.

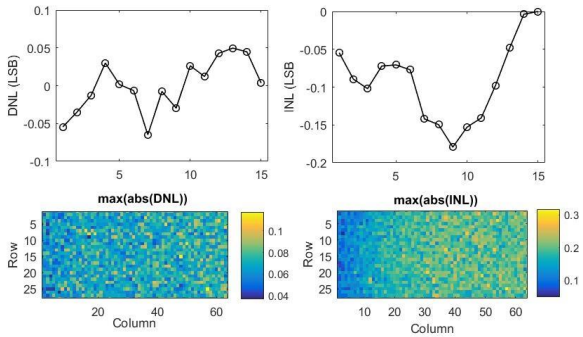

Fig. 15. Linearity in histogramming TDC mode

Fig. 15 shows a map of INL/DNL across the array taken by uniformly illuminating the image with uncorrelated light and performing a code density test. The linearity in this mode exceeds the few bits expected from the 16bins as the bin spacing is only dependent on clock edges within the shift register.

Fig. 16 shows the operation of the in-pixel counter based correlator with a threshold of 2 (a logic error prevents characterization of 4 and 8 thresholds). A 3.5 ns laser pulse is generated by an 840nm Picoquant Laser Diode at 3.8 MHz. A controlled background light level is generated by a blue 450 nm LED operated with 20 mA bias current causing the SPAD to operate around 900 kcps (measured in SPC mode). The TDC histograms are shown in single-shot timestamping mode with laser on in all cases for a single pixel with combinations of

DCR, background with and without correlator. The high background swamps the laser return in Fig. 16a making it indistinguishable from background. In Fig. 16b the correlator then reduces LED background by an order of magnitude and recovers the laser peak. In Fig. 16c.-d. the lower DCR level allows the laser peak to be seen and is then entirely suppressed by the correlator. A study of the degree of rejection of uncorrelated noise sources is given in [14] versus the coincidence level setting.

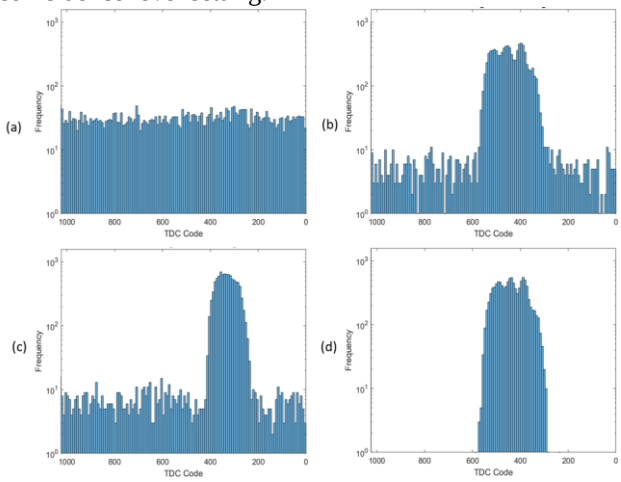

Fig. 16. Histograms in single shot TDC mode with LED background and 3.5ns pulsed laser on in all cases (a) DCR and LED background with correlator off (b) DCR and LED background with correlator on (c) DCR with correlator off (d) DCR with correlator on (DCR eliminated by correlator)

A 30 fps video of a subject waving 50 m away down a corridor in daylight conditions were taken with the previously mentioned 671 nm Picoquant laser setup using the in-pixel histogramming (Fig. 17). In this operating condition, the sensor consumes 77.6 mW including SPAD, GRO and digital core. The images are post-processed in Matlab software to calculate the centroid around the peak to generate real-time depth maps with low computational overhead. These calculations could readily be performed in FPGA or embedded on chip in a custom digital processor. Noisy pixels are removed by spatial filtering.

Fig. 18a and b detail two-step coarse-fine timings to allow the sensor to operate in a power efficient manner to deliver video ToF images at >50 m distances. In the scheme of Fig. 18a, the sensor uses only the multi-event histogramming mode. A first exposure is taken with a coarse 16 ns bin size to determine the four MSBs of the target range. Power consumption and jitter can be reduced by operating the METDC with an *Extclk* at 60 MHz and a laser rate of 3.9 MHz. In a second exposure, the laser rate is increased by 16x and the in-pixel GRO *TDCclk* generates the METDC clock tuned to 1GHz. This determines the next four LSBs of the target range but aliases the background.

The second timing approach in Fig. 18b achieves the same disambiguation by applying the single shot timestamping mode with the correlator prior to the short range METDC step. Here, the power consumption and accumulated jitter of the GRO can be minimized by operating with a *STOP* clock (60 MHz) at 16x laser repetition rate (3.9 MHz) and using the macro-time stamp feature to count STOP cycles. The second step is the same as in the first scheme using the METDC at 16 times the STOP rate. The METDC will alias photon returns outside the few meter bin ranges.

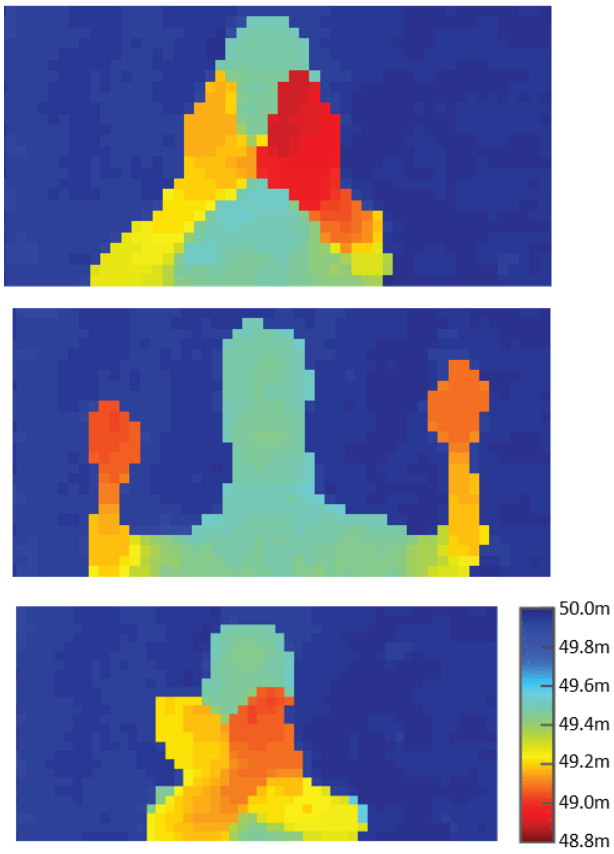

Fig. 17. Three images selected from a 30fps movie taken at 50m distance

The power consumption in corresponding modes is shown in Table 2. Global *Extclk* reduces power by a half over the same 60MHz frequency generated by the GRO while the correlator is able to reduce power by a third in single shot timestamping mode. A number of practical issues remain to be evaluated in terms of the real application of the proposed two step scheme. A few are the "stitching" of the two step images, associated motion blur, mismatch between the bin sizes, effect of noise and errors in MSB step on the LSB step especially for moving targets. These require quite extensive modelling and experimental work which is ongoing but beyond the immediate scope of this paper.

Fig. 19 shows the use of the global shutter histogramming mode to capture and freeze fast motion. Peak centroids are calculated real-time in Matlab software without any hot pixel removal or noise reduction. A pulsed laser source Picoquant LDH-Series 670 nm laser diode with ≈120 ps pulses at 60 MHz with 40 mW average optical power and a 3.5mm/f1.4 objective lens providing a 25 degree diagonal field of view have been used. An optical bandpass filter and a 1 ms exposure time are applied giving 60k laser repetitions per histogram. Example histograms with 560 ps bins are shown at several points in the image showing the possibility for multiple targets to be resolved where these fall across a single group of 4x4 SPADs.

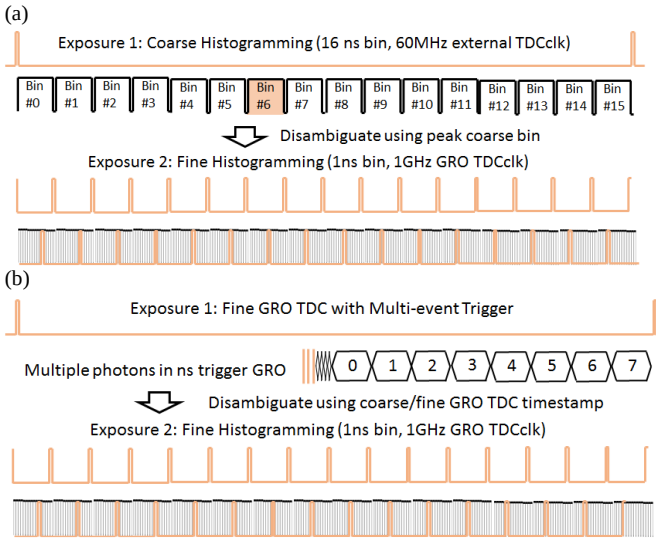

Fig. 18. Two proposed schemes to disambiguate short range (2m) histogramming over typical automotive (50m) LIDAR ranges.

	Histogram TDC Mode			Single Shot TDC Mode			
Scenario	GRO clock (60MHz)	Extclk (60MHz)	GRO clock (1 GHz)	DCR + No corr.	DCR + Corr + Laser	Bckgnd + Laser No Corr.	Bckgnd + Laser Corr.
VHV Power (mW)	36	36	36	0.13	0.18	0.88	0.9
V_{ddro} Power (mW)	66	0.8	6.8	0.67	0.64	0.61	0.64
V_{dd} Power (mW)	98.6	41.8	125	60.8	32.8	100.6	32.8

Table 2. Power consumption in the modes proposed in Fig. 18.

Parameters	Units	This Work	[8]	[9]	[10]	[2]
Sensor						
CMOS Technology	-	**90nm 1P4M/ 40nm 1P8M**	180nm	45nm/65nm	150nm	180nm
Pixel Array	-	**256x256/64x64**	252x144	16x8	64x64	16x1/32x1
Pixel Pitch	µm	**9.18/36.72**	28.5	19.8	60	21
Fill-factor	%	**51**	28	31.3/50.6	26.5	70
Median DCR@Veb	cps	**20@1.5V**	195 @5V	5.3k@2.5V	6.8k@3V	2.65k@NA
TDC depth	bits	**14/4**	12	14	16/15	12
TDC resolution	ps	**35/560**	48.8	60-320	250-20000	208
TDC area	μm^2	**130/150**	4200	550	NA	NA
TDC number	-	**4096**	1728	1	4096	64
TDC linearity DNL/INL	LSB	**+0.05/-0.05 +0.1/-0.08**	+0.6/-0.48 +0.89/-1.67	+0.8/-0.7 +3.4/-0.8	+1.2/-1 +4.8/-3.2	+0.15/-0.17 +0.32/-0.56
LIDAR Measurement						
Image resolution	-	**64x64**	252x144	256x256	64x64	202x96
Laser projection	-	**Flash**	Flash	Scanning	Flash	Scanning
Wavelength	nm	**671**	637	532	470	870
Repetition rate	MHz	**1.9**	40	1	NA	0.133
Mean illumination power	mW	**1.8**	2	6	NA	21
PDP@ illumination wavelength@Veb	%	**23@3V**	33.7@5V	21@2.5V	20@3V	NA
Max distance	m	**50**	50	150-430	367-5862	128
Imaging range	m	**50**	0.7	4.5	NA	100
FOV	deg.	**1.2x1.2**	40x20	NA	NA	
Accuracy	m(%)	**0.17(0.34)**	0.088(0.17)	0.07(0.3)	1.5(0.37)	11(0.11)
Background light	-	**1 klux**	dark	NA	100M/pix/s	70 klux
Target reflectivity	-	**white**	white	white	NA	9%
Power consumption	mW	**77.6**	2540	NA	93.5	530

Table 3. Comparison with the state of the art in SPAD sensors

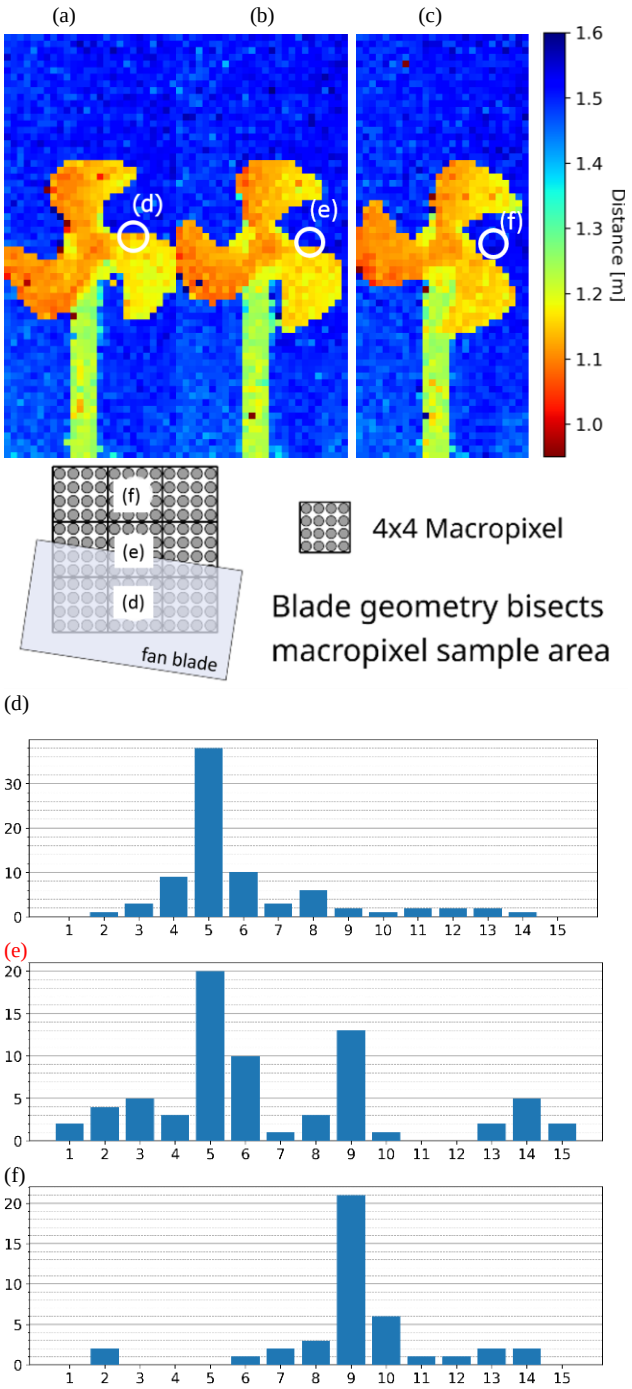

Fig. 19. Three consecutive ToF frames of a 1000 RPM fan taken at 380fps and 1ms exposure. Panel e shows distinct histogram peaks for both the fan blade edge and the backdrop, with adjacent points shown in panels e and f.

Table 3 compares this sensor with other recent advanced SPAD sensors. Our sensor is distinguished by low power consumption, high sensitivity and small pixel pitch as well as multi-mode imaging capability at a high dynamic range.

IV. Conclusion

It has been demonstrated that a compact SPAD pixel can be designed in advanced stacked-3D manufacturing technologies offering reconfigurable functionalities to reduce power and extend dynamic range enabling fast 3D imaging and flash LIDAR applications. Tradeoffs are made in the spatial and temporal resolution as well as sharing of resources amongst SPADs to achieve practical performance levels.

References

[1] R. Halterman and M. Bruch, "Velodyne HDL-64E lidar for unmanned surface vehicle obstacle detection," Proc. SPIE, Unmanned Syst. Technol. XII, vol. 7692, p. 76920D, May 2010,

[2] C. Niclass et al., "A 100-m Range 10-Frame/s 340 x 96-Pixel Time-of-Flight Depth Sensor in 0.18 μm CMOS," in IEEE JSSC, 2013.

[3] A. Eisele and R. Henderson, "185 MHz count rate, 139 dB dynamic range single-photon avalanche diode with active quenching circuit in 130nm CMOS technology," in Proc. Int. Image Sensor Workshop, 2011, pp. 6–8.

[4] T. A. Abbas et al., "Backside illuminated SPAD image sensor with 7.83μm pitch in 3D-stacked CMOS technology," IEDM 2016.

[5] S. Lhostis, A. Farcy, E. Deloffre, F. Lorut, S. Mermoz, Y. Henrion, L. Berthier, F. Bailly, D. Scevola, F. Guyader, F. Gigon, C. Besset, S. Pellissier, L. Gay, N. Hotellier, A. -L. Le Berrigo, S. Moreau, V. Balan, F. Fournel, A. Jouve, S. Ch´eramy, M. Arnoux, B. Rebhan, G. A. Maier and L. Chitu, "Reliable 300 mm Wafer Level Hybrid Bonding for 3D Stacked CMOS Image Sensors," 2016 IEEE 66th Electronic Components and Technology Conference (ECTC), Las Vegas, NV, 2016, pp. 869-876.

[6] S. Lindner, S. Pellegrini, Y. Henrion, B. Rae, M. Wolf, and E. Charbon, "A high-PDE, backside-illuminated SPAD in 65/40-nm 3D IC CMOS pixel with cascoded passive quenching and active recharge," IEEE Electron Device Lett., vol. 38, no. 11, pp. 1547–1550, Nov. 2017.

[7] M.-J. Lee and E. Charbon, "Progress in single-photon avalanche diode image sensors in standard CMOS: From two-dimensional monolithic to three-dimensional-stacked technology", Japanese Journal of Applied Physics 57, 1002A3 (2018)

[8] Zhang et al., "A 30-frames/s, 252 × 144 SPAD Flash LiDAR With 1728 Dual-Clock 48.8-ps TDCs, and Pixel-Wise Integrated Histogramming", IEEE J. Solid-State Circuits, Vol. 54, No. 4, pp. 1137-1151, April 2019

[9] A. Ximenes et al., "A 256×256 45/65nm 3D-stacked SPAD-based direct TOF image sensor for LiDAR applications with optical polar modulation for up to 18.6dB interference suppression", ISSCC 2018.

[10] M. Perenzoni et al., "A 64 x 64-Pixels Digital Silicon Photomultiplier Direct TOF Sensor With 100-MPhotons/s/pixel Background Rejection and Imaging/Altimeter Mode With 0.14% Precision Up To 6 km for Spacecraft Navigation and Landing," in IEEE JSSC, 2017.

[11] T. Al Abbas, D. Chitnis, F. Mattioli Della Rocca, R. K. Henderson, "Dual Layer 3D-Stacked High Dynamic Range SPAD Pixel", in Proceedings of IISW (IISS, 2019), pp. 206–209.

[12] I. Gyongy, S. W. Hutchings, M. Tyler, S. Chan, F. Zhu, R. K. Henderson, J. Leach, "1kFPS Time-of-Flight Imagng with a 3D-stacked CMOS SPAD Sensor", in Proceedings of IISW (IISS, 2019), pp. 226–229.

[13] N. A. W. Dutton et al., "11.5 A time-correlated single-photon-counting sensor with 14GS/S histogramming time-to-digital converter," ISSCC 2015.

[14] M. Beer et al. "Background Light Rejection in SPAD-Based LiDAR Sensors by Adaptive Photon Coincidence Detection." Sensors (Basel, Switzerland) vol. 18,12 4338. 8 Dec. 2018.

Author biographies will be available at time of publication.